Editors' Suggestion | Featured in Physics

Crossing $N = 28$ Toward the Neutron Drip Line: First Measurement of Half-Lives at FRIB

H. L. Crawford,[1,*] V. Tripathi,[2] J. M. Allmond,[3] B. P. Crider,[4] R. Grzywacz,[5] S. N. Liddick,[6,7] A. Andalib,[6,8] E. Argo,[6,8] C. Benetti,[2] S. Bhattacharya,[2] C. M. Campbell,[1] M. P. Carpenter,[9] J. Chan,[5] A. Chester,[6] J. Christie,[5] B. R. Clark,[4] I. Cox,[5] A. A. Doetsch,[6,8] J. Dopfer,[6,8] J. G. Duarte,[10] P. Fallon,[1] A. Frotscher,[1] T. Gaballah,[4] T. J. Gray,[3] J. T. Harke,[10] J. Heideman,[5] H. Heugen,[5] R. Jain,[6,8] T. T. King,[3] N. Kitamura,[5] K. Kolos,[10] F. G. Kondev,[9] A. Laminack,[3] B. Longfellow,[10] R. S. Lubna,[6] S. Luitel,[4] M. Madurga,[5] R. Mahajan,[6] M. J. Mogannam,[6,7] C. Morse,[11] S. Neupane,[5] A. Nowicki,[5] T. H. Ogunbeku,[4,6] W.-J. Ong,[10] C. Porzio,[1] C. J. Prokop,[12] B. C. Rasco,[3] E. K. Ronning,[6,7] E. Rubino,[6] T. J. Ruland,[13] K. P. Rykaczewski,[3] L. Schaedig,[6,8] D. Seweryniak,[9] K. Siegl,[5] M. Singh,[5] S. L. Tabor,[2] T. L. Tang,[2] T. Wheeler,[6,8] J. A. Winger,[4] and Z. Xu[5]

[1]*Nuclear Science Division, Lawrence Berkeley National Laboratory, Berkeley, California 94720, USA*
[2]*Department of Physics, Florida State University, Tallahassee, Florida 32306, USA*
[3]*Physics Division, Oak Ridge National Laboratory, Oak Ridge, Tennessee 37831, USA*
[4]*Department of Physics and Astronomy, Mississippi State University, Mississippi State, Mississippi 39762, USA*
[5]*Department of Physics and Astronomy, University of Tennessee, Knoxville, Tennessee 37966, USA*
[6]*Facility for Rare Isotope Beams, Michigan State University, East Lansing, Michigan 48824, USA*
[7]*Department of Chemistry, Michigan State University, East Lansing, Michigan 48824, USA*
[8]*Department of Physics and Astronomy, Michigan State University, East Lansing, Michigan 48824, USA*
[9]*Argonne National Laboratory, Argonne, Illinois 60439, USA*
[10]*Lawrence Livermore National Laboratory, Livermore, California 94550, USA*
[11]*Brookhaven National Laboratory, Upton, New York 11973, USA*
[12]*Los Alamos National Laboratory, Los Alamos, New Mexico 87545, USA*
[13]*Department of Physics and Astronomy, Louisiana State University, Baton Rouge, Louisiana 70803, USA*

(Received 19 July 2022; accepted 14 September 2022; published 14 November 2022)

New half-lives for exotic isotopes approaching the neutron drip-line in the vicinity of $N \sim 28$ for $Z =$ 12–15 were measured at the Facility for Rare Isotope Beams (FRIB) with the FRIB decay station initiator. The first experimental results are compared to the latest quasiparticle random phase approximation and shell-model calculations. Overall, the measured half-lives are consistent with the available theoretical descriptions and suggest a well-developed region of deformation below ^{48}Ca in the $N = 28$ isotones. The erosion of the $Z = 14$ subshell closure in Si is experimentally confirmed at $N = 28$, and a reduction in the ^{38}Mg half-life is observed as compared with its isotopic neighbors, which does not seem to be predicted well based on the decay energy and deformation trends. This highlights the need for both additional data in this very exotic region, and for more advanced theoretical efforts.

DOI: 10.1103/PhysRevLett.129.212501

Introduction.—The neutron-proton imbalance in nuclei far from the valley of β stability is ultimately responsible for the neutron drip line—the limit of existence beyond which the nuclear system with an additional neutron is not bound. Slightly closer to stability, in bound exotic nuclei, the same neutron excess affects the detailed impacts of the residual nuclear interaction, modifying single-particle energies and potentially leading to altered ground- and excited-state properties as compared with stable isotopes [1,2]. The ability to predict the impacts and effects of large neutron excess is central to the study of nuclear structure and nucleosynthesis and relies on advancing both theory and experiment.

The Facility for Rare Isotope Beams (FRIB) has recently begun operations and will provide access to thousands of nuclei far from stability, many for the first time. These rare isotope beams will enable measurements necessary to understand the properties of exotic nuclei and how the elements are synthesized. Here, we report on first data from FRIB where the energy and intensity of the ^{48}Ca primary beam offered unique access to exotic isotopes approaching the neutron drip line in the vicinity of $N = 28$. The Mg, Al, and Si isotopes in the neutron-rich $N \sim 28$ region are an ideal laboratory to study the changes in single-particle structure and (sub)shell closures as well as collective degrees of freedom that occur due to the large neutron-proton asymmetry. It is currently the highest mass region experimentally accessible up to the neutron drip line, where there is also the potential for weak binding to impact nuclear structure properties, most dramatically seen in the formation of extended neutron radii, or halos.

Leveraging the sensitivity of β decay and the FRIB Decay Station initiator (FDSi) [3,4], new half-lives were measured in the most neutron-rich P, Si, Al and Mg isotopes. While ultimately the most stringent tests of theory will come from detailed measurements, half-lives are a key

 © 2022 American Physical Society

experimental quantity, the systematics of which can provide important insight into the evolution of structure across the nuclear chart. This experiment extends the previous decay work in this region [5,6] by several neutrons for these key isotopic chains between $Z = 12$–15, including values for five previously unreported cases up to and crossing $N = 28$. These new data show clear evidence for the erosion of the $Z = 14$ subshell closure at $N = 28$, and an intriguing reduction in half-life for the most neutron-rich Mg isotope relative to its lighter isotopic neighbors.

Experiment.—A primary beam of ^{48}Ca was accelerated through the three segments of the FRIB linac to a final energy of 172.3 MeV/u. The fully stripped ~1 kW (120 particle-nA) $^{48}Ca^{20+}$ beam then impinged on a 8.89 mm ^{9}Be fragmentation target, producing a broad range of secondary isotopes. The preseparator selected nuclei with a $B\rho$ of 5.100 Tm, based on the optimum production energy for ^{42}Si. Additional stages of separation through the Advanced Rare Isotope Separator (ARIS) [7] selected a cocktail beam centered around ^{42}Si after passing through a wedge and degrader foil. The fragments were delivered to the FDSi at a rigidity of 4.904 Tm.

The FDSi was installed in the FRIB transfer hall, just 2.5 m beyond the exit of the primary switching magnet. The setup is built around a 5 mm thick fast-response YSO (yttrium orthosilicate, Y_2SiO_5) scintillator implantation detector [8] that was segmented into 48×48 1 mm $\times$ 1 mm elements, which were connected to a 16×16 glass light guide leading to an H12700 Hamamatsu 8×8 multianode photomultiplier. Surrounding the implantation detector, the FDSi as deployed for this experiment included 11 HPGe clover detectors and 15 fast-timing $LaBr_3$ detectors mounted in one hemisphere on the north side of the implantation detector. On the south side, 88 neutron detectors of the VANDLE [9,10] array were installed in two layers at flight distances of 90 and 96 cm from the implantation detector. Two large-area Si PIN detectors (100 cm^2 and 40 cm^2) and a 2 mm thick plastic scintillator were positioned approximately 1.5 m upstream of the implantation detectors in the last diagnostic detector box of the beamline. Two additional plastic scintillator veto detectors sandwiched the YSO implantation detector. An Al degrader was used to implant the ions, from F to P in this 5 mm YSO.

The cocktail beam delivered to the FDSi is shown in the particle identification plot in Fig. 1, where ions are identified event by event by energy loss in the upstream PIN detector (Z determination) and time of flight between a 6 μm plastic timing scintillator at the start of stage 3 of the ARIS separator and the timing scintillator in the diagnostic detector box immediately upstream of the implantation detector (A/Q determination) over a flight path of 33.5 m.

All of the individual detectors of the FDSi were read out using XIA Pixie16 digitizers, and built into events based on a global timestamp shared between all modules with a

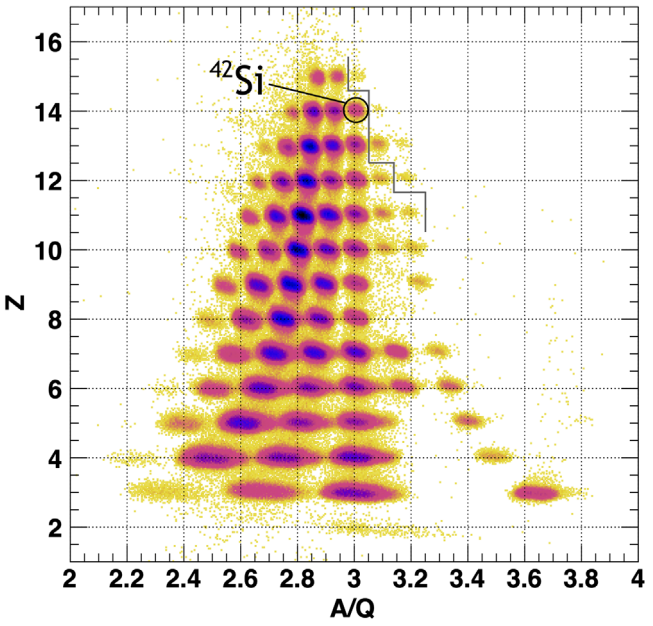

FIG. 1. Particle identification plot for the cocktail of heavy ions delivered to the FDSi in the present experiment. Z was determined based upon the energy loss in the upstream PIN detector(s), while the A/Q is derived from $B\rho$ and the time of flight as described in the text. The five newly measured half-lives are to the right of the solid gray line from $Z = 12$–15.

10 μs event window. Implanted ions were identified as those events for which the low-gain signal of the YSO was present, in addition to signals in the upstream PIN detectors and timing scintillator. Implant positions were derived event by event based on four position signals (anodes) and a common dynode signal, using Anger logic [11]. The electronics scheme included 10× amplification for the high-gain signal as described in more detail in Ref. [12]. Decay events were identified as events for which a high-gain signal was detected in the implantation detector, and no signal was detected in any of the upstream detectors or veto detectors on either side of the YSO. The plastic scintillators were essential to reject light particles, which otherwise generated background in the β spectrum. Positions were derived for all such events, and correlated based on temporal and position information with previous implants. Time correlations for the present analysis were defined within a maximum time window of 150 ms between an implant and all subsequent decay events.

Results.—The decay curves for ^{44,45}P, ^{42,43}Si, ^{40,41}Al, and ^{37,38}Mg are given in Fig. 2. The half-life for each isotope was obtained by fitting the decay curves to a function that considered the decay of the parent, the exponential growth and decay of the daughter(s), including potential βn and $\beta 2n$ decay branches; and a constant background. Information on the half-lives of the daughter(s) and β-delayed neutron emission probabilities was taken from the literature [13], or guided by the calculations of Ref. [14] where experimental data were not available. Table I

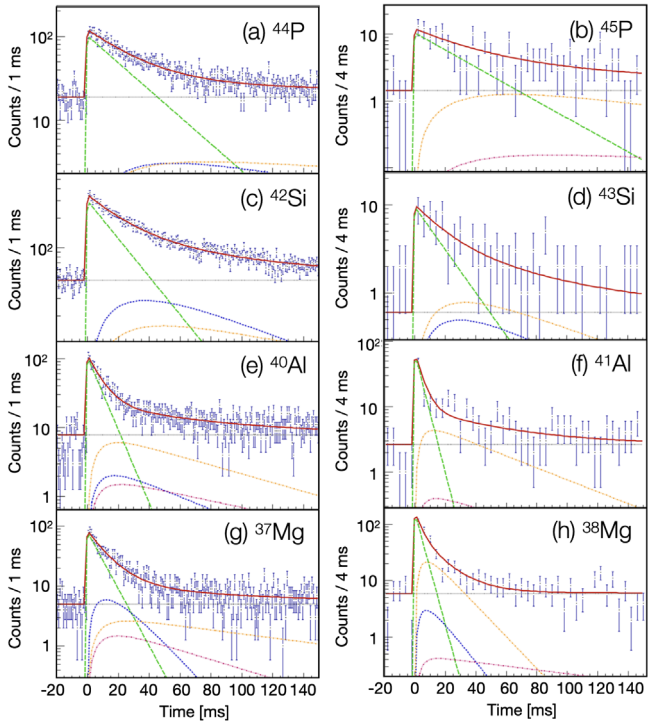

FIG. 2. Decay curves in panels (a)–(h) for ^{44,45}P, ^{42,43}Si, ^{40,41}Al, and ^{37,38}Mg respectively. The components of the fits are shown by the curves, where the solid red line is the total fit, the green dashed curve is the parent decay, the dot-dash blue line is the $\beta 0n$ daughter contribution, the dot-dot-dash orange line is the $\beta 1n$ contribution, the dot-dot-dot-dash magenta line is the $\beta 2n$ contribution, and the dotted gray line is the constant background. The derived half-lives are included in Table I.

summarizes the statistics of the present measurement and the assumptions made in the half-life fitting. Fit parameters were determined based on a binned maximum likelihood fitting procedure. The statistical error was determined by the error on the fit parameter. A systematic error was also determined, which accounts for the variation in the central value of the derived half-life when varying input assumptions, particle gates, and/or correlation times. This includes varying daughter half-lives within their quoted uncertainties, and varying β-delayed neutron emission probabilities by $\pm 100\%$ of the value in Table I.

The extracted half-lives and previously measured literature values (where available) are included in the last columns of Table I. Also included are the half-lives derived in the present Letter for ^{35}Na, ^{32}Ne, and ^{29}F. All values are in good agreement with the literature values. These cases give confidence in the experimental sensitivity for very short half-lives in this measurement.

The case of ^{36}Mg requires one additional comment. The half-life of the $\beta 0n$ daughter, ^{36}Al, is reported in the literature as 90(40) ms [13]. However, a more recent measurement suggests a much shorter ground-state half-life of 12.2(10) ms [19], with a longer-lived β-decaying isomeric state in ^{36}Al. The half-life reported assumes the published half-life, but the systematic error bar in this case encompasses the results of a fit assuming the much shorter daughter half-life.

Discussion.—The experimental half-lives for the neutron-rich P, Si, Al, and Mg isotopes are plotted in the panels of Fig. 3. The current results are shown by the filled symbols, while the evaluated half-lives [13] are indicated by the open symbols. Also included in each plot are the calculated β-decay half lives, evaluated within a number of different approaches as discussed below.

Among the most complete compilations of calculated nuclear properties are those performed in the framework of the quasiparticle random phase approximation (QRPA). As such, QRPA calculations are frequently used to make predictions regarding the most exotic nuclei and as input to astrophysical models, such as r-process network calculations. Given their frequent use, it is interesting to compare the current half-life data with QRPA predictions. Möller *et al.* [14] compiled ground-state properties of nuclides across the nuclear chart from ^{16}O to ^{339}136, including QRPA-calculated decay rates with nuclear deformations based on the finite-range droplet model and folded Yukawa single-particle potential [22]. Half-lives are calculated from Gamow-Teller (GT) decay rates, combined with a phenomenological treatment of first-forbidden (FF) decays. These calculations are included as the dotted lines for each isotope in the top panel of Fig. 3.

The QRPA framework accounts for certain aspects of nuclear structure such as deformation, allowing insight to be gained from systematic behavior and comparison with data. That said, the QRPA calculations are not expected to capture the more subtle microscopic evolution of structure, nor the potential impacts of the continuum approaching the neutron drip line. This is apparent in the comparison with data—while the general trends are reasonably well reproduced for the P, Si, Al, and Mg isotopes, the degree of odd-even staggering and behavior at $N = 20$ and $N = 28$ do not agree with the data.

For calculations which may capture the microscopic aspects of nuclei in this region, one can turn to large-scale shell-model calculations. Yoshida *et al.* [20] performed such calculations using an extension of the SDPF-MU effective interaction [23] into the $sd + pf + sdg$ valence space for the very neutron-rich Al, Si, and P isotopes. The SDPF-MU interaction has been very successful in the description of the low-lying level structure for these isotopic chains approaching $N = 28$, while the expanded valence space allows for consideration of both GT and FF transitions in the decay.

The results of these shell-model calculations, using experimental Q_β values, are shown as the dashed lines in the lower panel of Fig. 3 for the Al, Si, and P isotopes. The agreement with data for all three isotopic chains is excellent up to, and across $N = 28$, reproducing very well

TABLE I. Correlation statistics and the deduced half-lives for the neutron-rich isotopes studied in the present Letter. Correlated decays include multiple generations of decays and all β-delayed neutron branches.

	Parent nuclei statistics		Fit assumptions		$T_{1/2}$ (ms)	
Nuclide	Implants	Correlated decays	$P_{\beta 0n,\beta 1n,\beta 2n}$ (%)	$T_{1/2}^{\beta 0n,\beta 1n\beta 2n}$ (ms)	This Letter	Previous
^{44}P	5116	6427	24/55/21	100/265/1013	$18.8(8)_{\mathrm{stat}}(15)_{\mathrm{sys}}$	18.5(2.5)[a] [5,6]
^{45}P	159	188	0/79/21[c]	68/100/265	$24(7)_{\mathrm{stat}}(9)_{\mathrm{sys}}$	⋯
^{42}Si	11419	18495	51/48/1	48.5/101/150	$15.5(4)_{\mathrm{stat}}(16)_{\mathrm{sys}}$	12.5(3.5)[a] [6]; 20(10) [15]
^{43}Si	63	99	27/52/21	36.5/48.5/101	$13(4)_{\mathrm{stat}}(2)_{\mathrm{sys}}$	⋯
^{39}Al	53436	95511	3/94/3[b]	47.5/63/90	$7.22(8)_{\mathrm{stat}}(30)_{\mathrm{sys}}$	7.6(1.6)[a] [6]; 8(2) [15]
^{40}Al	1632	2824	16/64/20[c]	33/47.5/63	$5.7(3)_{\mathrm{stat}}(2)_{\mathrm{sys}}$	⋯
^{41}Al	133	255	3/86/11[c]	20/33/47.5	$3.5(8)_{\mathrm{stat}}(4)_{\mathrm{sys}}$	⋯
^{36}Mg	40933	82640	52/48/0[b]	90/38.2/56.3	$7.2(1)_{\mathrm{stat}}(12)_{\mathrm{sys}}$	$7.6(^{+5}_{-8})$ [16]; 3.9(1.3)[a] [6]; ∼5 [15]
^{37}Mg	1027	2055	27/57/16	10.7/90/38.2	$6.4(4)_{\mathrm{stat}}(14)_{\mathrm{sys}}$	8(4)[a] [15]
^{38}Mg	265	556	9/81/9	9.0/10.7/90	$3.1(4)_{\mathrm{stat}}(2)_{\mathrm{sys}}$	⋯
^{35}Na	377	813	14/73/10	11.3/20/92	$2.4(3)_{\mathrm{stat}}(2)_{\mathrm{sys}}$	1.5(5)[a] [17]
^{32}Ne	652	1449	21/75/4	13.2/17.4/48	$4.5(4)_{\mathrm{stat}}(6)_{\mathrm{sys}}$	3.5(9)[a] [18]
^{29}F	899	2104	40/50/10[b]	14.7/18.8/30.9	$3.4(4)_{\mathrm{stat}}(1)_{\mathrm{sys}}$	2.5(3)[a] [13]

[a]Corresponds to the adopted half-life value [13].
[b]$P_{\beta xn}$ include experimental constraints: $P_{\beta xn}^{x\geq 1}$ for ^{39}Al, ^{36}Mg, and ^{29}F, are 97(22)%, 48(12)%, and 60(40)%, respectively [13].
[c]$P_{\beta xn}$ include experimental constraints from lighter isotopes: $P_{\beta xn}^{x\geq 1}$ for ^{45}P, ^{40}Al and ^{41}Al are 100% (from ^{43}P), 84(19)% (from ^{38}Al) and 97(22)% (from ^{39}Al), respectively [13].

the newly measured values and capturing the nuclear structure at a microscopic level as compared with QRPA. For the Mg isotopes, large-scale shell-model predictions for the β-decay half-lives are not reported with the SDPF-MU family of interactions. The only recent shell-model prediction available for the Mg isotopes uses the WBMB [24] effective interaction [21]. While this interaction has been successful in the region of $N = 20$, it is not considered as broadly applicable for the more neutron-rich isotopes approaching $N = 28$. Indeed, as is shown in the bottom panel of Fig. 3, the calculated half-lives of Ref. [21] for the Mg isotopes are systematically higher than experiment and do not provide good agreement. Once the required valence space can be handled by large-scale shell-model calculations updated predictions using the SDPF-MU family of interactions will be extremely interesting for the Mg isotopes.

Stepping back from the detailed comparisons with theory, the systematics of the experimental half-life data alone provide significant insight into the structure of isotopes in the *sd-pf* shell. First, the slopes of the P/Si chains relative to the Mg/Al chains are substantially different. The Mg and Al isotopes follow a shallower trend with neutron number, which is consistent with the 2_1^+ energy systematics and the interpretation of the Mg isotopes as a chain of deformed nuclei extending from $N = 20$ at least to $N = 26$ [25]. The difference in the slopes of Al and Si isotopic chains also highlights the evolution of the $Z = 14$ subshell closure. At $N = 20$, there is a clear gap in the half-lives of the Si and Al isotones, with a difference of more than 1 order of magnitude. This is consistent with the interpretation of $Z = 14$ as a subshell closure in ^{34}Si [26]. However, as N is increased, the Si and Al half-lives converge, indicating the erosion of the proton subshell closure approaching $N = 28$. This is consistent with previous experimental information [27,28] and with the predictions of the SDPF-MU shell-model calculations, which include significant deformation in the $N = 28$ isotones and the disappearance of the spherical $Z = 14$ subshell closure. The newly measured half-lives extend the systematics and provide additional experimental confirmation of this picture.

Finally, we note the drop in half-life measured in the current work for ^{38}Mg compared with the neighboring ^{37}Mg and lighter isotopes. The systematics of the first two excited states in the even-even Mg isotopes [25] suggest a fairly stable deformation from $N = 20$ to $N = 26$, excluding changing deformation as a mechanism to explain the change in half-life. A local fit to the lighter Mg isotopes assuming an approximate Q_β^{-5} dependence as expected by Gross β-decay theory [29] suggests that Q_β is also not a driver for this drop; however, the uncertainty on the Q values is too large to completely exclude this possibility. As highlighted by this Letter, improved nuclear masses in this region are needed to provide more precise Q_β values. Furthermore, how the proximity to the drip line approaching $N = 28$ influences beta decay is not known, and a determination of the ^{40}Mg half-life will be of great interest to help resolve this question. Insight from the predictions of the shell-model in this region will be invaluable, but remains a challenge. Not only is a large valence space required to capture the relevant excitations, but continuum coupling effects may become increasingly important for near drip line cases.

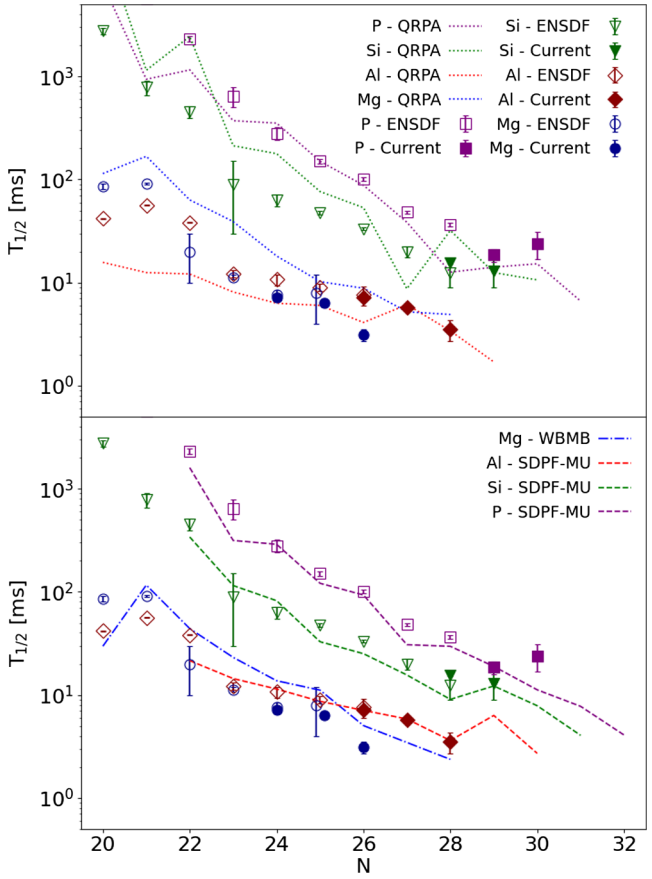

FIG. 3. Systematics for the half-lives ($T_{1/2}$) of the P, Si, Al, and Mg isotopic chains as a function of neutron number, N. The evaluated half-lives from the literature [13] are represented by the open symbols, while the present results are represented by filled symbols in purple squares, green triangles, red diamonds and blue circles for P, Si, Al, and Mg, respectively. For $^{37}Mg_{25}$ the literature and present results are offset horizontally for visual clarity only. The top panel also includes the results from the QRPA calculation of Ref. [14] as dotted lines for each isotopic chain, while the lower panel includes as dashed lines the results of large-scale shell-model calculations [20] using the SDPF-MU effective interaction for P, Si, and Al. Also included in the bottom panel are the results of shell-model calculations [21] using the WBMB effective interaction for Mg, as a blue dot-dashed line.

Conclusion.—β-decay half-lives of exotic neutron-rich Mg, Al, Si, and P isotopes in the vicinity of $N \sim 28$ were measured using the FDSi at FRIB. This measurement extends the available data by several neutrons for these key isotopic chains between $Z = 12$ and $Z = 15$ and includes five previously unreported cases up to and crossing $N = 28$. The new data show clear evidence for the erosion of the $Z = 14$ subshell closure at $N = 28$, in agreement with theoretical predictions and an intriguing reduction in half-life for the neutron-rich ^{38}Mg isotope relative to its isotopic neighbors, a result which awaits extension of the large-scale shell-model calculations to the Mg chain. The experiment was the first to be carried out at the newly constructed Facility for Rare Isotope Beams and already demonstrates the advanced capabilities and new science opportunities to come as the facility develops toward its full beam intensity of 400 kW.

We would like to thank the entire operations team at FRIB for their amazing work in beam delivery during the experiment, and for all of the work leading up to this measurement. This material is based upon work supported in part by the U.S. Department of Energy, Office of Science, Office of Nuclear Physics under Contracts No. DE-AC02-06CH11357 (ANL), No. DE-AC02-98CH10946 (BNL), No. DE-AC02-05CH11231 (LBNL), No. DE-AC52-07NA27344 (LLNL), No. DE-SC0020451 (Michigan State), No. DE-SC0014448 (Mississipi State), No. DE-AC05-00OR22725 (ORNL), and No. DE-FG02-96ER40983 (UTK). This work was also supported by the U.S. National Science Foundation under Grants No. PHY-2012522 (FSU) and No. PHY-1848177 (CAREER) (Mississippi State). The research was also sponsored by the U.S. Department of Energy, National Nuclear Security Administration under Award No. DE-NA0003180 (Michigan State) and the Stewardship Science Academic Alliances program through DOE Awards No. DE-NA0003899 (UTK) and No. DOE-DE-NA0003906 (Michigan State), and NSF Major Research Instrumentation Program Award No. 1919735 (UTK).

*Corresponding author.
hlcrawford@lbl.gov

[1] T. Otsuka, A. Gade, O. Sorlin, T. Suzuki, and Y. Utsuno, Rev. Mod. Phys. **92**, 015002 (2020).
[2] O. Sorlin and M.-G. Porquet, Prog. Part. Nucl. Phys. **61**, 602 (2008).
[3] Frib decay station initiator proposal (2020), https://fds.ornl.gov/wp-content/uploads/2020/09/FDSi-Proposal-May2020.pdf.
[4] Frib decay station initiator (2022), https://fds.ornl.gov/initiator/.
[5] S. Grvy, J. Mrazek, J. Anglique, P. Baumann, C. Borcea, A. Buta, G. Canchel, W. Catford, S. Courtin, J. Daugas *et al.*, Nucl. Phys. **A722**, C424 (2003).
[6] S. Grvy, J. Anglique, P. Baumann, C. Borcea, A. Buta, G. Canchel, W. Catford, S. Courtin, J. Daugas, F. de Oliveira *et al.*, Phys. Lett. B **594**, 252 (2004).
[7] M. Hausmann, A. Aaron, A. Amthor, M. Avilov, L. Bandura, R. Bennett, G. Bollen, T. Borden, T. Burgess, S. Chouhan *et al.*, Nucl. Instrum. Methods Phys. Res., Sect. A **317**, 349 (2013).
[8] R. Yokoyama, M. Singh, R. Grzywacz, A. Keeler, T. King, J. Agramunt, N. Brewer, S. Go, J. Heideman, J. Liu *et al.*, Nucl. Instrum. Methods Phys. Res., Sect. A **937**, 93 (2019).
[9] S. Paulauskas, M. Madurga, R. Grzywacz, D. Miller, S. Padgett, and H. Tan, Nucl. Instrum. Methods Phys. Res., Sect. A **737**, 22 (2014).

[10] W. Peters, S. Ilyushkin, M. Madurga, C. Matei, S. Paulauskas, R. Grzywacz, D. Bardayan, C. Brune, J. Allen, J. Allen *et al.*, Nucl. Instrum. Methods Phys. Res., Sect. A **836**, 122 (2016).
[11] H. O. Anger, Rev. Sci. Instrum. **29**, 27 (1958).
[12] M. Singh *et al.* (to be published).
[13] F. Kondev, M. Wang, W. Huang, S. Naimi, and G. Audi, Chin. Phys. C **45**, 030001 (2021), and references therein.
[14] P. Mller, M. Mumpower, T. Kawano, and W. Myers, At. Data Nucl. Data Tables **125**, 1 (2019).
[15] K. Yoneda, H. Sakurai, N. Aoi, N. Fukuda, T. Gomi, E. Ideguchi, N. Imai, H. Iwasaki, T. Kubo, Z. Liu *et al.*, RIKEN Accel. Prog. Rep. **32**, 78 (1999).
[16] K. Steiger, Ph.D. thesis, Technischen Universität München (2013).
[17] M. Langevin, C. Detraz, D. Guillemaud-Mueller, A. Mueller, C. Thibault, F. Touchard, and M. Epherre, Phys. Lett. **125B**, 116 (1983).
[18] M. Notani, N. Aoi, N. Fukuda, H. Iwasaki, K. Yoneda, H. Ogawa, T. Teranishi, S. M. Lukyanov, Y. E. Penionzhkevich, T. Nakamura *et al.*, AIP Conf. Proc. **455**, 359 (1998).
[19] R. S. Lubna (private communication).
[20] S. Yoshida, Y. Utsuno, N. Shimizu, and T. Otsuka, Phys. Rev. C **97**, 054321 (2018).
[21] H. Li and Z. Ren, J. Phys. G **40**, 105110 (2013).
[22] P. Mller, A. Sierk, T. Ichikawa, and H. Sagawa, At. Data Nucl. Data Tables **109–110**, 1 (2016).
[23] Y. Utsuno, T. Otsuka, B. A. Brown, M. Honma, T. Mizusaki, and N. Shimizu, Phys. Rev. C **86**, 051301(R) (2012).
[24] E. K. Warburton, J. A. Becker, and B. A. Brown, Phys. Rev. C **41**, 1147 (1990).
[25] P. Doornenbal, H. Scheit, S. Takeuchi, N. Aoi, K. Li, M. Matsushita, D. Steppenbeck, H. Wang, H. Baba, H. Crawford *et al.*, Phys. Rev. Lett. **111**, 212502 (2013).
[26] P. Baumann, A. Huck, G. Klotz, A. Knipper, G. Walter, G. Marguier, H. Ravn, C. Richard-Serre, A. Poves, and J. Retamosa, Phys. Lett. B **228**, 458 (1989).
[27] B. Bastin, S. Grévy, D. Sohler, O. Sorlin, Z. Dombrádi, N. L. Achouri, J. C. Angélique, F. Azaiez, D. Baiborodin, R. Borcea *et al.*, Phys. Rev. Lett. **99**, 022503 (2007).
[28] S. Takeuchi, M. Matsushita, N. Aoi, P. Doornenbal, K. Li, T. Motobayashi, H. Scheit, D. Steppenbeck, H. Wang, H. Baba *et al.*, Phys. Rev. Lett. **109**, 182501 (2012).
[29] B. Pfeiffer, K.-L. Kratz, and P. Mller, Prog. Nucl. Energy **41**, 39 (2002).